ISSN 0020-1685, Inorganic Materials, 2016, Vol. 52, No. 10, pp. 1077–1084. © Pleiades Publishing, Ltd., 2016.
Original Russian Text © E.V. Dedyaeva, T.K. Akopyan, A.G. Padalko, G.V. Talanova, G.I. Zubarev, A.D. Izotov, A.N. Suchkov, V.T. Fedotov, L.I. Shvorneva, 2016, published in Neorganicheskie Materialy, 2016, Vol. 52, No. 10, pp. 1148–1155.

High-Pressure Phase Transitions and Structure of Al–20 at % Si Hypereutectic Alloy

E. V. Dedyaeva[a], T. K. Akopyan[a], A. G. Padalko[a, *], G. V. Talanova[a], G. I. Zubarev[b], A. D. Izotov[c], A. N. Suchkov[d], V. T. Fedotov[d], and L. I. Shvorneva[a]

[a] *Baikov Institute of Metallurgy and Materials Science, Russian Academy of Sciences, Leninskii pr. 49, Moscow, 119991 Russia*
[b] *OAO United Engine Corporation, pr. Budennogo 16, Moscow, 105118 Russia*
[c] *Kurnakov Institute of General and Inorganic Chemistry, Russian Academy of Sciences, Leninskii pr. 31, Moscow, 119991 Russia*
[d] *National Nuclear Research University MIFI (Moscow Engineering Physics Institute), Kashirskoe sh. 31, Moscow, 115409 Russia*
**e-mail: padalko@inbox.ru*

Received May 22, 2015; in final form, February 10, 2016

Abstract—Phase transformations of an Al–20 at % Si high-silicon hypereutectic alloy have been studied by differential barothermal analysis at temperatures of up to 800°C in argon compressed to 100 MPa. High pressure has been shown to raise the melting point of the alloy by 5°C during heating and to lower the eutectic solidification temperature by 5°C during cooling in comparison with the canonical phase diagram of the Al–Si system. At a temperature of 553°C, heating and cooling lead to silicon dissolution and decomposition of the aluminum-based solid solution, respectively. After high-pressure solidification, the silicon particles in the alloy have a bimodal size distribution. Quantitative porosity characteristics in the alloy after a barothermal scanning cycle are similar to those in the as-prepared alloy. The lattice parameters of the silicon and aluminum remain unchanged. The microhardness of the aluminum matrix of the alloy corresponds to that of pure aluminum.

Keywords: differential barothermal analysis, pressure, silumin, microstructure
DOI: 10.1134/S002016851610006X

INTRODUCTION

Combining a large number of valuable properties, such as low density, sufficiently good mechanical properties at elevated temperatures, and technological feasibility for casting, welding, and various types of mechanical processing, alloys based on the Al–Si binary system (silumins) are widely used in modern machine building. Silumins with various chemical compositions and, accordingly, with various microstructures include tens of commercially viable materials [1] which are used as various components of internal combustion engines and many other gears and machines. The mechanical properties of cast silumins and the performance parameters of silumin-based products can be further improved by varying their chemical composition, adjusting heat-treatment conditions, and modifying them with the aim of optimizing their microstructure (so-called metallurgical approach). On the other hand, the properties of the alloys can be significantly improved by eliminating micropores of various origins and homogenizing their chemical composition through barothermal processing (hot isostatic pressing (HIP)), in which a material is simultaneously subjected to high pressures and temperatures [2, 3]. This ensures densification of the material to near theoretical densities through plastic deformation, followed by diffusion-assisted bonding of the joined inner surfaces of the pores. Sufficiently active diffusion processes at elevated temperatures and pressures ensure significant homogenization of the elemental composition, which was made inhomogeneous by segregation processes during solidification of the cast material.

Note that successful preparation of any alloys, including those based on the Al–Si system, is impossible without detailed, accurate phase diagram data for binary metallic systems that can be considered canonical [4, 5]. At the same time, canonical phase diagrams were obtained in studies of phase transformations in binary systems at atmospheric pressure, which introduces a degree of uncertainty when elevated pressures are used in barothermal processing. This circumstance is associated with the fact that the well-known Clapeyron–Clausius thermodynamic equation, which relates

the pressure-induced change in the temperature of a transformation to the associated molar volume change under equilibrium conditions, was obtained for unary systems, whereas industrial alloys contain at least three chemical elements, and up to 10–15 elements in the case of high-temperature nickel alloys [6]. Because of this, a theoretical analysis of the pressure-induced shift of characteristic temperatures of binary and more complex alloys presents serious difficulties, so experimental work in this direction is of great current interest and importance [7].

The first studies concerned with high-pressure phase diagrams of the binary system Al–Si include those by Fujishiro et al. [8] and Mii et al. [9], who investigated a number of compositions in the composition range 0–15 at % Si at two fixed pressures, 5.46 [8] and 2.5 GPa [9], and obtained liquidus, solidus, and solvus curves using electrical resistance measurements to detect phase transformations. Pressure was applied using an anvil system at a small sample volume. It is worth noting that their results are undoubtedly of fundamental importance but, because of the extremely high pressure range and very small sample weight, they are beyond the barothermal processing parameters commonly employed in modern practice of HIP, which uses pressures within 200 MPa, rarely up to 300 MPa, with the weight of the material reaching (2–3) × 10^3 kg. The purpose of this work was to study phase transformations in Al–Si alloys, in particular in a 20 at % Si + 80 at % Al alloy, at a pressure of ~100 MPa in a compressed argon atmosphere using quantitative microstructural analysis, X-ray diffraction, and scanning electron microscopy.

EXPERIMENTAL

Thermal events were examined using a differential thermal analysis cell placed in the high-pressure chamber of a HIP system (ABRA, Switzerland) [10, 11]. The alloy synthesis conditions and sample preparation procedure were described in sufficient detail elsewhere [12–14]. Microstructures were examined first on an MeF3 optical microscope (Austria) equipped with a digital imaging accessory and a high-pressure mercury lamp, which allowed features down to ~0.5 μm to be imaged. Higher resolution images were obtained by scanning electron microscopy (SEM) on a Leo 1500 instrument (Carl Zeiss, Germany). Images were obtained in backscatter mode at an accelerating voltage of 20 kV or using SiK_α X-ray mapping. X-ray diffraction measurements were made on a Rigaku Ultima IV diffractometer (nickel-filtered CuK_α radiation, D/teX high-resolution linear position-sensitive detector). Data were analyzed using PDXL integrated X-ray diffraction analysis software, incorporating the PDF-2 database. For quantitative analysis, PDXL relies on the reference intensity ratio method (corundum standard) [20]. Vickers microhardness tests were performed on a PMT-3 microhardness tester (OAO LOMO, Russia) by a standard procedure. To improve microstructure imaging quality and obtain quantitative information about the microstructural constituents of the alloy, images were analyzed with Adobe Photoshop CS6 and ImageJ, respectively, and experimental data sets were analyzed with Origin 5.0 software.

RESULTS AND DISCUSSION

The as-prepared alloy, synthesized by melting Al and Si powders, had a microstructure that was formed during substantially nonequilibrium crystallization in the solidification process during filling of a quartz capillary tube ~4 mm in diameter (Figs. 1a, 1b). At low magnifications (Fig. 1a), the structure of the alloy is characterized by large primary silicon dendrite crystals up to 400 μm in size, arranged at random in the bulk of the mini-ingot, and by a coarse, needle-like (Al) + Si binary eutectic (Figs. 1b, 1c), with the silicon needles ranging in length from 100 to 150 μm.

The synthesized alloy had considerable porosity, localized in the aluminum-based solid solution (Figs. 1c, 1d), whereas the silicon particles were free of such structural defects. Using image processing (Fig. 1d) with appropriate software, we obtained the histogram of the pore size distribution presented in Fig. 2. In constructing the histogram, the minimum pore diameter was limited to 0.5 μm, which was the resolving power of the MeF3 microscope used.

Quantitative porosity characteristics were as follows: total porosity, 10.4 vol %; average pore diameter, 1.2 μm; average pore volume, 9.6 × 10^{-13} cm^3; pore number density, 2.7 × 10^{10} cm^{-3}. The histogram was well represented by the relation

$$N^0_{\text{pore}} = 1.7 \times 10^3 e^{-3.7d}, \quad (1)$$

where N^0_{pores} is the number of pores in the as-prepared material and d (μm) is the pore diameter.

A sample with the above characteristics of its microstructural constituents, weighing ~100 mg, was loaded into a differential thermal analysis (DTA) cell placed in the high-pressure chamber of the HIP system.

Differential barothermal analysis (DBA). In our experiments, the argon pressure in the high-pressure chamber was first brought to ~50 MPa. Next, the system was heated at a constant rate of 8°C/min. In accordance with the relation $pV = nRT$, the linear heating was accompanied by a linear rise in pressure (1 MPa/min) in the chamber. At the temperatures of

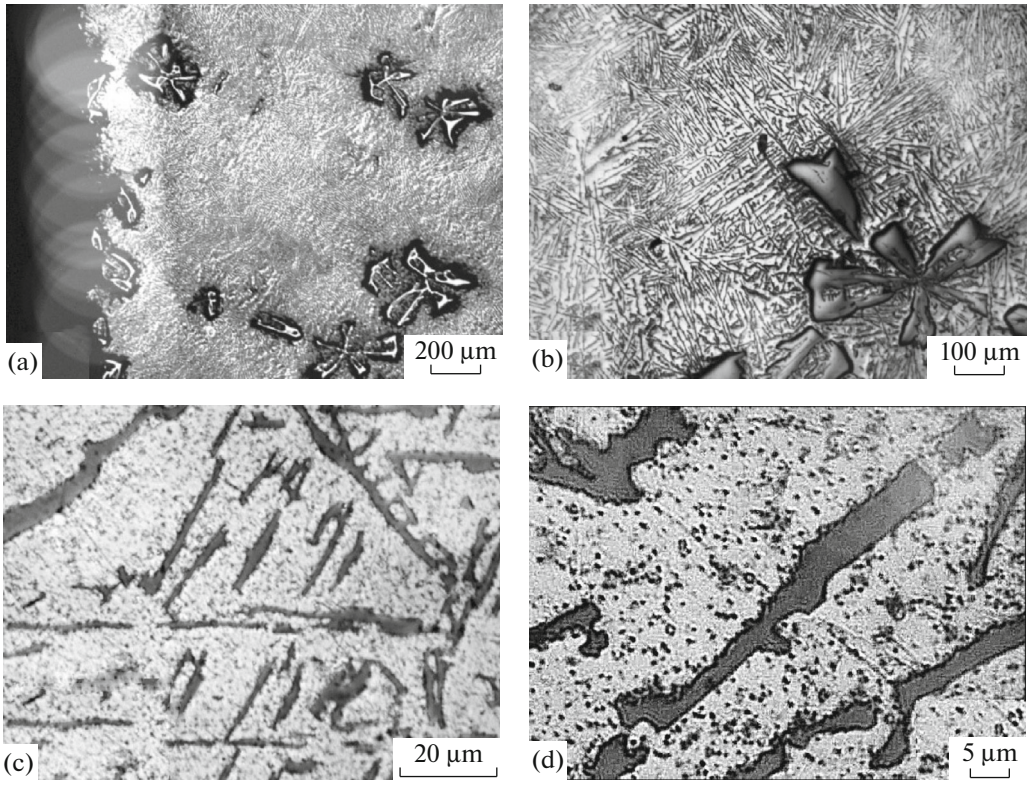

Fig. 1. Microstructure of the as-prepared Al–20 at % Si alloy (optical microscopy): (a) primary Si crystals, (b) eutectic and primary Si crystals in the (Al) matrix, (c) pores in the (Al) matrix and eutectic Si crystals, (d) unprocessed image for quantitative characterization of porosity.

the phase transformations, the compressed argon pressure reached 100 ± 2 MPa. Our barothermal experiments each consisted of a single heating/cooling cycle, as is typical of thermal analysis, and provided reliable information about the temperatures of high-pressure phase transformations.

In the DBA heating curve (Fig. 3, curve *1*), we identified four heat effects. The weak endothermic peak at 553°C is due to the dissolution of eutectic and primary silicon crystals in the aluminum matrix. The process is thermodynamically driven: according to previous findings [4, 9], increasing the silicon concentration in aluminum leads to a linear decrease in its lattice parameter and the corresponding decrease in its unit-cell volume. Thus, silicon dissolution in aluminum under uniform pressure is a thermodynamically favorable process. The strongest peak arises from the melting of the Al + Si eutectic. The $S \rightarrow L$ transformation process begins at 582°C, which is 5°C above the melting point of the eutectic at atmospheric pressure [4, 5]. The peak at 693°C corresponds to the completion of the melting of the alloy, that is, to the liquidus temperature of the alloy, which is essentially identical to that in the canonical equilibrium Al–Si phase diagram [5], despite the applied pressure of 100 MPa. The insensitivity of the liquidus temperature to pressure can be accounted for by the extremely small change in specific volume upon melting, because most of the silicon melts during heating from the eutectic temperature (solidus) to the liquidus temperature, and the melting of the rest of the silicon has a weak effect on

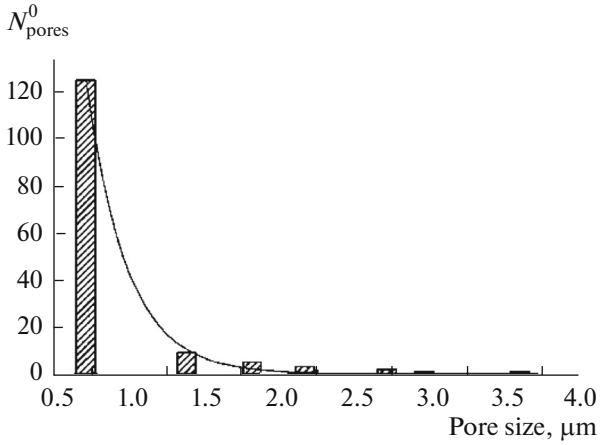

Fig. 2. Histogram of the pore size distribution in the as-prepared Al–20 at % Si alloy.

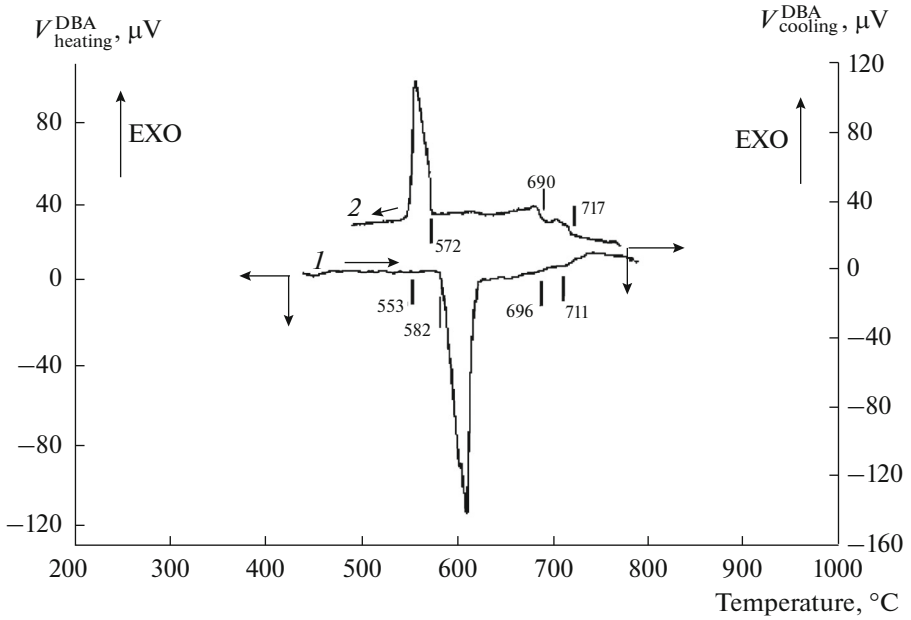

Fig. 3. DBA curves of the Al–20 at % Si alloy at 100 MPa: (*1*) heating, (*2*) cooling.

the change in the density of the melt. The peak at 720°C arises from liquid-phase processes. The mechanism of the transformation involved is described in detail below.

In the DBA cooling curve (Fig. 3, curve *2*), we identified three exothermic peaks. At 718°C, the temperature of the sample in the liquid phase was observed to rise. In discussing this effect, attention should be given to structural studies of liquid phases in the binary system Al–Si [15] and in the Al–Si–Ni system [16]. Their results demonstrate that, at temperatures slightly above the liquidus temperature, the melt in the binary system Al–Si is a heterogeneous system (emulsion) in which some of the silicon present in the alloy has the form of ordered particles ranging in size from 1 to 10 nm [15]. Under the assumption that the particles are spherical in shape, this means that the number of unit cells per particle is 8 to 8000. X-ray diffraction data for an Al–Si–Ni alloy [16] also point to partial ordering of the liquid phase, which was interpreted in terms of the formation of Al_3Ni and AlNi intermetallic particles. Thus, the exothermic peak at 718°C in the cooling curve and the endothermic peak at 720°C in the heating curve are attributable to silicon particle disintegration processes during melt heating and particle coagulation during cooling of the sample.

Eutectic crystallization begins at 572°C, which is 5°C below the eutectic temperature of the alloy at atmospheric pressure. The decrease in the eutectic crystallization temperature relative to the melting point can be accounted for by both usual melt supercooling and "thermodynamic" supercooling, which is determined by the transition of the system to a less dense state upon the precipitation of silicon particles from the melt and by the decrease in the density of the alloy. Note that the pressure coefficients for the melting points of pure Al were reported to be ~5.6 [8, 9] and 6.5°C/100 MPa [15], whereas the solidus temperature (eutectic melting point) of the Al–20 at % Si alloy in argon compressed to 100 MPa increases on heating with a reduced pressure coefficient of 5°C/100 MPa. In the case of the two-phase alloy under study, this can be accounted for by the fact that the densities of aluminum and silicon change in opposite ways upon melting (the density of aluminum decreases, whereas that of silicon rises), resulting in a small increase in the specific volume of the crystallizing alloy.

Lowering the temperature of the system would be expected to lead to the precipitation of silicon particles as a result of the decomposition of the supersaturated (Al) solid solution. Because of its small heat effect, the temperature of this transformation was determined by plotting the time derivative of a differential cooling curve (Fig. 4), which clearly showed an inflection at 553°C, suggesting a considerable decrease in the cooling rate of the sample because of the heat release during the precipitation of silicon particles.

A significant distinction of the data obtained in a DBA cycle (Fig. 5) from canonical data is the solid-state precipitation of silicon nanoparticles at 553°C,

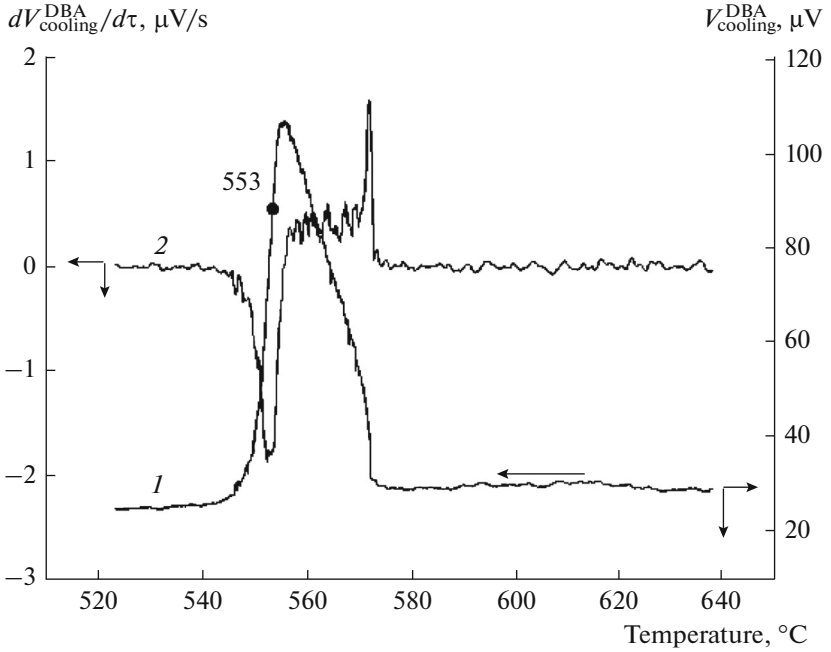

Fig. 4. (*1*) DBA cooling curve at 100 MPa and (*2*) its time derivative for the Al–20 at % Si alloy.

which is of obvious interest for practical applications in barothermal processing of silumins.

The DBA cycle reduced the micropore density in the alloy to 2.2×10^{10} cm^{-3} and increased the average pore diameter to 1.3 μm and, accordingly, the average pore volume to 1.2×10^{-12} cm^3, resulting in a slight increase in the volume fraction of pores: to 10.6 vol % (table). Figure 6 shows the histogram of the pore size distribution obtained from analysis of the image in Fig. 7c.

The awnalytical expression for the pore size distribution in the alloy after the DBA cycle has the form

$$N^{DBA}_{pores} = 2.7 \times 10^2 e^{-2.3d}, \quad (2)$$

where N^{DBA}_{pores} is the number of pores in the material after the DBA cycle and d (μm) is the pore diameter.

In this formula, the pre-exponential factor, which is determined by the total number of pores under consideration, and the exponent are smaller than those for

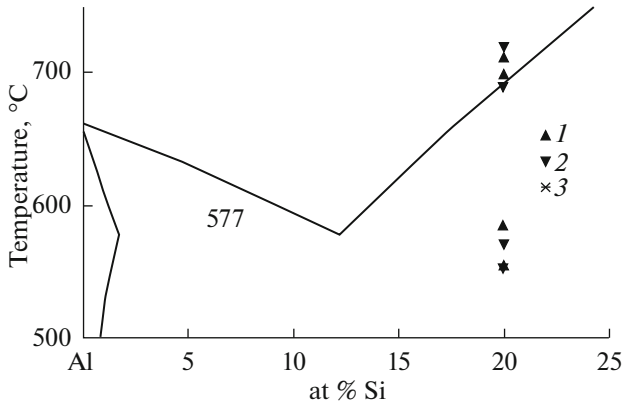

Fig. 5. Portion of the canonical equilibrium phase diagram of the binary system Al–Si [4, 5] with experimental DBA data for the Al–20 at % Si alloy at 100 MPa: (*1*) heating, (*2*) cooling, (*3*) identical data points obtained during heating and cooling.

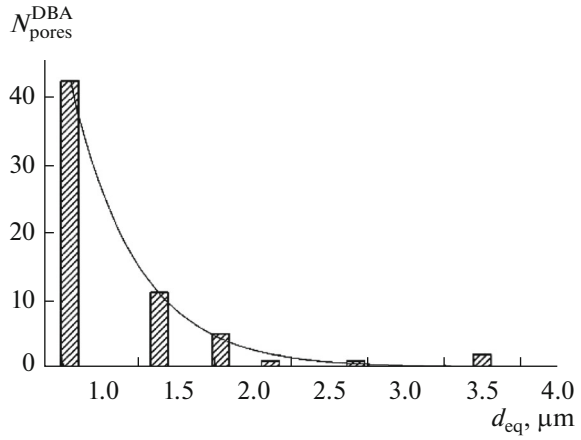

Fig. 6. Histogram of the pore size distribution in the Al–20 at % Si alloy after a DBA cycle at 100 MPa.

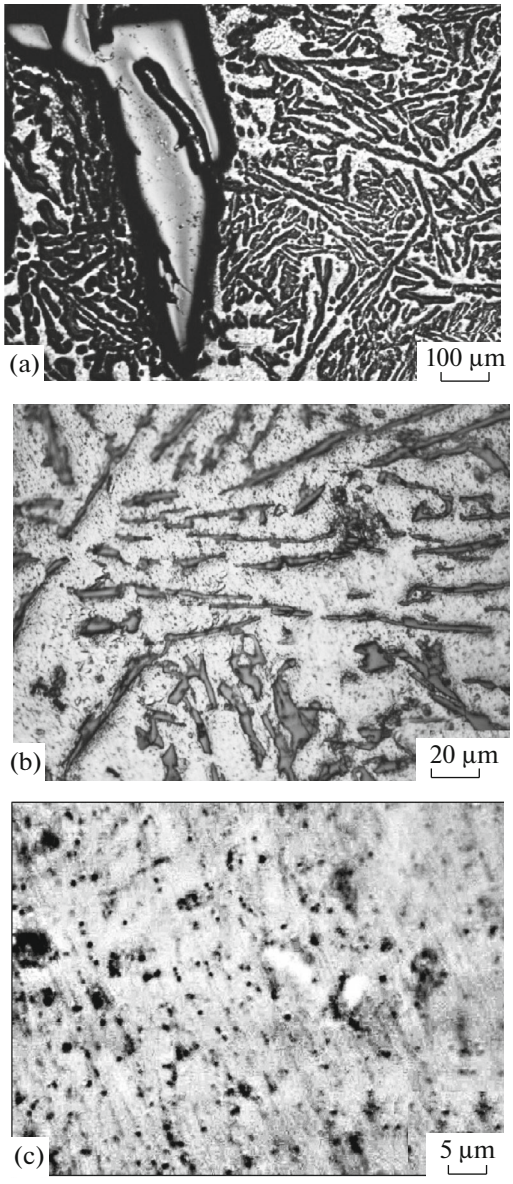

Fig. 7. Microstructure of the Al–20 at % Si alloy after a DBA cycle at 100 MPa: (a) primary Si crystal and eutectic silicon, (b) eutectic Si crystals in the (Al) matrix, (c) unprocessed image for quantitative characterization of porosity.

the as-prepared alloy, which points to a broader pore size distribution.

The porosity data for the alloy before and after DBA are presented in the table.

It follows from the table that the quantitative porosity characteristics in the as-prepared alloy are essentially identical to those after the DBA cycle, which is attributable to grain-boundary argon diffusion to the pores during heating of the alloy, until the argon pressure in the pores reaches the external pressure, and the reverse process during cooling of the alloy. The analytical expression (2) indicates that the number of pores becomes a weaker function of pore size.

The microstructure of the alloy solidified at 100 MPa (Figs. 7a, 7b) is considerably coarser than that of the as-prepared alloy. The eutectic silicon particles typically have needle-like morphology, with an inclusion length in the range 400–500 μm and a cross-sectional size of the needles from 3 to 7 μm. The observed changes in the morphology of the microstructural constituents of the alloy are due to the slow cooling rate in our barothermal experiments and the nearly zero-gradient crystallization conditions in the DTA cell.

The morphology of the fine silicon particles was examined in greater detail by SEM. Backscattered electron images were found to have low contrast and, accordingly, low resolution.

To identify small silicon particles in the aluminum matrix, we used $\mathrm{Si}K_{\alpha_1}$ X-ray maps, which were further analyzed with Adobe Photoshop CS6. In Fig. 8b, one can see that large eutectic silicon crystals are surrounded by finely dispersed silicon precipitates. With the technique used, we were unable to determine the size of the small silicon particles, but it is reasonable to assume that their size lies in the submicron range. Such particles most likely originate from solid-state (Al) decomposition, which occurs at 553°C (Fig. 4, curve *2*).

The X-ray diffraction pattern of the Al–20 at % Si alloy shows only reflections from aluminum and silicon (Fig. 9a). The silicon content estimated using PDXL is 13.5%, which is lower than the intended Si content and the Si content deduced from DBA data. One possible reason for this is that reflections from silicon microparticles surrounded by submicron silicon particles have reduced intensity (Fig. 8b). The possibility of such an effect in quantitative X-ray diffraction analysis was examined by Kovba and Trunov [19]. Further, the peaks in the silicon 422 doublet were assumed to be superpositions of reflections from silicon particles of various sizes, as suggested by SEM results (Fig. 8b). Larger particles then determine the intensity of the peaks in the $\mathrm{Cu}K_{\alpha_1}/\mathrm{Cu}K_{\alpha_2}$ 422 doublet, and fine silicon particles are responsible for the broadening of the base of the peaks in the doublet. 422 doublet decomposition results demonstrate that the overall composite peak can rather adequately be decomposed into four components differing in intensity and full width at half maximum (Fig. 9b). Qualitatively, this suggests that the silicon particles have a bimodal size distribution, in agreement with the above SEM data. The lattice parameters of the silicon microparticles and aluminum, as determined using PDXL, are almost identical to those indicated in the ICDD PDF database.

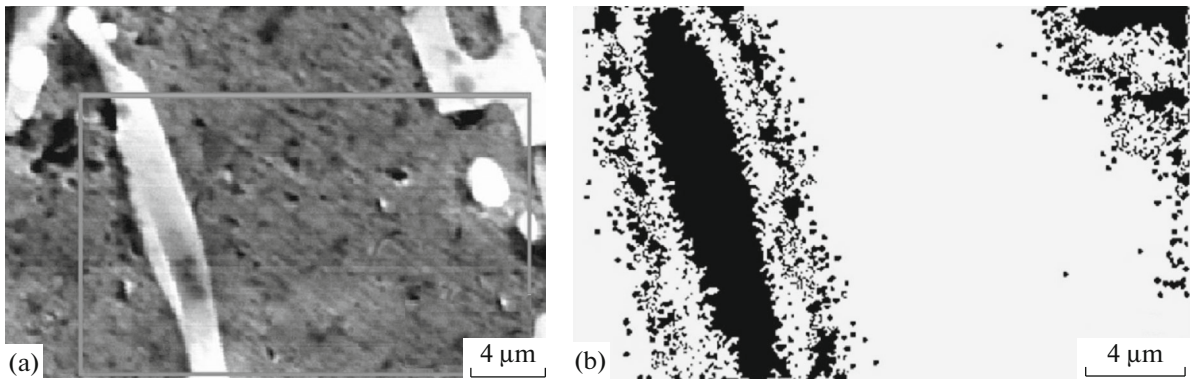

Fig. 8. Microstructure of the Al–20 at % Si alloy: (a) backscattered electron image, (b) SiK_{α_1} X-ray map after image processing.

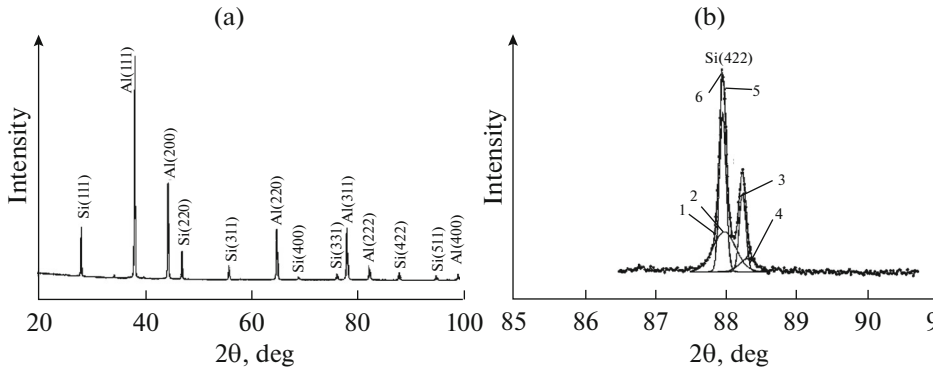

Fig. 9. (a) X-ray diffraction pattern of the Al–20 at % Si alloy solidified at 100 MPa; (b) Si(422) peak decomposition results: peaks 1 and 2 are reflections from silicon nanoparticles and microparticles, respectively, in CuK_{α_1} radiation; peaks 3 and 4 are reflections from silicon nanoparticles and microparticles, respectively, in CuK_{α_2} radiation; peaks 5 and 6 are the sum of peaks 1–4 and the observed X-ray diffraction profile, respectively.

The Vickers microhardness of the aluminum matrix in the alloy crystallized at high pressure was measured at an indentation load of 0.1 N and a dwell time of 15 s. Under these conditions, the indent diagonal did not exceed 40 μm and the indent edges were at least 30–40 μm away from Si microcrystals. The average microhardness of (Al) thus determined is 156 MPa, which correlates well with the microhardness of pure aluminum [18].

CONCLUSIONS

Phase transformations of an Al–20 at % Si alloy have been studied by DBA at temperatures of up to 700°C in argon compressed to 100 MPa. The eutectic temperature was found to increase by 5°C. The DBA cooling curve of the alloy showed a small heat effect at 553°C, which was attributed to the decomposition of the aluminum-based solid solution and precipitation

Quantitative porosity characteristics in the Al–20 at % Si alloy

Alloy	Pore number density, 10^{10} cm^{-3}	Average pore diameter, μm	Average pore volume, 10^{-12} cm^3	Volume fraction of pores, %	Exponent*
As-prepared	2.7	1.2	0.96	10.4	$-3.7d$
After DBA	2.2	1.3	1.2	10.6	$-2.3d$

* See formulas (1) and (2).

of submicron silicon particles. After high-pressure solidification, the silicon particles in the alloy had a bimodal size distribution.

A barothermal scanning cycle has little effect on quantitative porosity characteristics in the alloy. The lattice parameters of the silicon and aluminum remain unchanged. The microhardness of the aluminum matrix of the alloy corresponds to that of pure aluminum.

ACKNOWLEDGMENTS

This work was supported by the Russian Foundation for Basic Research (grant no. 11-03-00689-a) and the Chemistry and Materials Science Division of the Russian Academy of Sciences (basic research program).

REFERENCES

1. Prigunova, A.G., Belov, N.A., Taran, Yu.N., Zolotorevskii, V.S., Napalkov, V.I., and Petrov, S.S., *Siluminy. Atlas mikrostruktur i fraktogramm promyshlennykh splavov (Silumins: Atlas of Microstructures and Fracture Surface Maps for Industrial Alloys)*, Moscow: Mosk. Inst. Stali i Splavov, 1996.
2. Westerlund, J. and Vimercati, A., Four decades of HIP progress, *Met. Powd. Rep.,* 2000, vol. 55, no. 2, pp. 14–21.
3. Padalko, A.G., *Praktika goryachego izostaticheskogo pressovaniya neorganicheskikh materialov (Practical Issues in Hot Isostatic Pressing of Inorganic Materials)*, Moscow: Akademkniga, 2007.
4. Murray, J.L. and McAlister, A.J., The Al–Si (aluminum–silicon) system, *Bull. Alloy Phase Diagrams,* 1984, vol. 5, no. 1, pp. 74–84.
5. *Diagrammy sostoyaniya dvoinykh metallicheskikh sistem. Spravochnik* (Phase Diagrams of Binary Metallic Systems: A Handbook), Lyakishev, N.P., Ed., Moscow: Mashinostroenie, 1996, 1997, 2001, vols. 1–3.
6. Kablov, E.N. and Golubovskii, E.R., *Zharoprochnost' nikelevykh splavov (High-Temperature Strength of Nickel Alloys)*, Moscow: Mashinostroenie, 2005.
7. Glazov, V.M., Chizhevskaya, S.N., and Glagoleva, N.N., *Zhidkie poluprovodniki (Liquid Semiconductors)*, Moscow: Nauka, 1967.
8. Fujishiro, I., Mii, H., Senoo, M., and Akao, M., High pressure phase diagram of Al–Si system, *J. Soc. Mater. Sci. Jpn.,* 1971, no. 20, pp. 952–955.
9. Mii, H., Senoo, M., and Fujishiro, I., Solid solubility of Si in Al under high pressure, *Jpn. J. Appl. Phys.,* 1976, no. 15, pp. 777–783.
10. Padalko, A.G., Veselov, A.N., Avduhin, S.P., et al., Differential barothermal analysis (DBA) of Ni-base alloys, *J. Therm. Anal. Calorim.,* 2003, vol. 72, no. 3, pp. 791–797.
11. Padalko, A.G., Belov, N.A., Veselov, A.N., and Talanova, G.V., Thermography of the phase transformations in a hypoeutectic Al–7% Si–0.5% Mg silumin at high pressures and temperatures, *Russ. Metall. (Engl. Transl.),* 2009, no. 1, pp. 65–60.
12. Padalko, A.G., Talanova, G.V., Zubarev, G.I., Fedotov, V.T., Suchkov, A.N., and Tsarev, V.I., Thermography of the phase transformations in nickel-based eutectic alloys at high pressures and temperatures, *Russ. Metall. (Engl. Transl.),* 2011, no. 3, 169–174.
13. Padalko, A.G., Talanova, G.V., Ponomareva, E.Yu., Talyat-Kelpsh, V.V., Shvorneva, L.I., Zubarev, G.I., Fedotov, V.T., Suchkov, A.N., and Baklan, V.A., Phase transformations at high pressures and temperatures and the structure of a hypoeutectic 1Ni–99Al alloy, *Russ. Metall. (Engl. Transl.),* 2012, no. 9, pp. 779–785.
14. Padalko, A.G., Talanova, G.V., Ponomareva, E.Yu., Talyat-Kelpsh, V.V., Shvorneva, L.I., Zubarev, G.I., Fedotov, V.T., Suchkov, A.N., and Baklan, V.A., Barothermal analysis and structure of the eutectic Al–Ni (2.7 at % Ni) alloy, *Inorg. Mater.,* 2012, vol. 48, no. 6, pp. 582–587.
15. Zhukova, L.A., Aksenova, O.P., and Zamyatin, V.M., Enthalpy increment of a hypoeutectic Al–Si alloy during heating in solid and liquid states, *Rasplavy,* 2004, no. 2, pp. 36–39.
16. Mudry, S. and Shtablavyi, I., Cluster structure in Al–Si eutectic melt with solid Ni particles, *Chem. Met. Alloys,* 2008, no. 1, pp. 163–167.
17. Tonkov, E.Yu., *Fazovye prevrashcheniya soedinenii pri vysokom davlenii (High-Pressure Phase Transformations of Compounds)*, Moscow: Metallurgiya, 1988, vols. 1–2.
18. Properties of aluminum. Handbook of Nonferrous Metals. http://www.libmetal.ru/al/al%20prop.htm.
19. Kovba, L.M. and Trunov, V.K., *Rentgenofazovyi analiz (X-Ray Diffraction Analysis)*, Moscow: Mosk. Gos. Univ., 1976.
20. Hubbard, C.R., Evans, E.H., and Smith, D.K., The reference intensity ratio, I/I_c, for computer simulated powder patterns, *J. Appl. Crystallogr.,* 1976, vol. 9, pp. 169–174.

Translated by O. Tsarev